This paper is published as part of a PCCP Themed Issue on:

Modern EPR Spectroscopy: Beyond the EPR Spectrum

Guest Editor: Daniella Goldfarb

Editorial

Modern EPR spectroscopy: beyond the EPR spectrum
Phys. Chem. Chem. Phys., 2009
DOI: 10.1039/b913085n

Perspective

Molecular nanomagnets and magnetic nanoparticles: the EMR contribution to a common approach
M. Fittipaldi, L. Sorace, A.-L. Barra, C. Sangregorio, R. Sessoli and D. Gatteschi, *Phys. Chem. Chem. Phys.*, 2009
DOI: 10.1039/b905880j

Communication

Radiofrequency polarization effects in zero-field electron paramagnetic resonance
Christopher T. Rodgers, C. J. Wedge, Stuart A. Norman, Philipp Kukura, Karen Nelson, Neville Baker, Kiminori Maeda, Kevin B. Henbest, P. J. Hore and C. R. Timmel, *Phys. Chem. Chem. Phys.*, 2009
DOI: 10.1039/b906102a

Papers

Radiofrequency polarization effects in low-field electron paramagnetic resonance
C. J. Wedge, Christopher T. Rodgers, Stuart A. Norman, Neville Baker, Kiminori Maeda, Kevin B. Henbest, C. R. Timmel and P. J. Hore, *Phys. Chem. Chem. Phys.*, 2009
DOI: 10.1039/b907915g

Three-spin correlations in double electron–electron resonance
Gunnar Jeschke, Muhammad Sajid, Miriam Schulte and Adelheid Godt, *Phys. Chem. Chem. Phys.*, 2009
DOI: 10.1039/b905724b

^{14}N HYSCORE investigation of the H-cluster of [FeFe] hydrogenase: evidence for a nitrogen in the dithiol bridge
Alexey Silakov, Brian Wenk, Eduard Reijerse and Wolfgang Lubitz, *Phys. Chem. Chem. Phys.*, 2009
DOI: 10.1039/b905841a

Tyrosyl radicals in proteins: a comparison of empirical and density functional calculated EPR parameters
Dimitri A. Svistunenko and Garth A. Jones, *Phys. Chem. Chem. Phys.*, 2009
DOI: 10.1039/b905522c

General and efficient simulation of pulse EPR spectra
Stefan Stoll and R. David Britt, *Phys. Chem. Chem. Phys.*, 2009
DOI: 10.1039/b907277b

Dynamic nuclear polarization coupling factors calculated from molecular dynamics simulations of a nitroxide radical in water
Deniz Sezer, M. J. Prandolini and Thomas F. Prisner, *Phys. Chem. Chem. Phys.*, 2009
DOI: 10.1039/b905709a

Dynamic nuclear polarization of water by a nitroxide radical: rigorous treatment of the electron spin saturation and comparison with experiments at 9.2 Tesla
Deniz Sezer, Marat Gafurov, M. J. Prandolini, Vasyl P. Denysenkov and Thomas F. Prisner, *Phys. Chem. Chem. Phys.*, 2009
DOI: 10.1039/b906719c

Dynamic mixing processes in spin triads of "breathing crystals" Cu(hfac)$_2$L^R: a multifrequency EPR study at 34, 122 and 244 GHz
Matvey V. Fedin, Sergey L. Veber, Galina V. Romanenko, Victor I. Ovcharenko, Renad Z. Sagdeev, Gudrun Klihm, Edward Reijerse, Wolfgang Lubitz and Elena G. Bagryanskaya, *Phys. Chem. Chem. Phys.*, 2009
DOI: 10.1039/b906007c

Nitrogen oxide reaction with six-atom silver clusters supported on LTA zeolite
Amgalanbaatar Baldansuren, Rüdiger-A. Eichel and Emil Roduner, *Phys. Chem. Chem. Phys.*, 2009
DOI: 10.1039/b903870a

Multifrequency ESR study of spin-labeled molecules in inclusion compounds with cyclodextrins
Boris Dzikovski, Dmitriy Tipikin, Vsevolod Livshits, Keith Earle and Jack Freed, *Phys. Chem. Chem. Phys.*, 2009
DOI: 10.1039/b903490k

ESR imaging in solid phase down to sub-micron resolution: methodology and applications
Aharon Blank, Ekaterina Suhovoy, Revital Halevy, Lazar Shtirberg and Wolfgang Harneit, *Phys. Chem. Chem. Phys.*, 2009
DOI: 10.1039/b905943a

Multifrequency EPR study of the mobility of nitroxides in solid-state calixarene nanocapsules
Elena G. Bagryanskaya, Dmitriy N. Polovyanenko, Matvey V. Fedin, Leonid Kulik, Alexander Schnegg, Anton Savitsky, Klaus Möbius, Anthony W. Coleman, Gennady S. Ananchenko and John A. Ripmeester, *Phys. Chem. Chem. Phys.*, 2009
DOI: 10.1039/b906827a

Ferro- and antiferromagnetic exchange coupling constants in PELDOR spectra
D. Margraf, P. Cekan, T. F. Prisner, S. Th. Sigurdsson and O. Schiemann, *Phys. Chem. Chem. Phys.*, 2009
DOI: 10.1039/b905524j

Electronic structure of the tyrosine D radical and the water-splitting complex from pulsed ENDOR spectroscopy on photosystem II single crystals
Christian Teutloff, Susanne Pudollek, Sven Keßen, Matthias Broser, Athina Zouni and Robert Bittl, *Phys. Chem. Chem. Phys.*, 2009
DOI: 10.1039/b908093g

A W-band pulsed EPR/ENDOR study of $Co^{II}S_4$ coordination in the $Co[(SPPh_2)(SP^iPr_2)N]_2$ complex
Silvia Sottini, Guinevere Mathies, Peter Gast, Dimitrios Maganas, Panayotis Kyritsis and Edgar J.J. Groenen, *Phys. Chem. Chem. Phys.*, 2009
DOI: 10.1039/b905726a

Exchangeable oxygens in the vicinity of the molybdenum center of the high-pH form of sulfite oxidase and sulfite dehydrogenase
Andrei V. Astashkin, Eric L. Klein, Dmitry Ganyushin, Kayunta Johnson-Winters, Frank Neese, Ulrike Kappler and John H. Enemark, *Phys. Chem. Chem. Phys.*, 2009
DOI: 10.1039/b907029j

Magnetic quantum tunneling: key insights from multi-dimensional high-field EPR
J. Lawrence, E.-C. Yang, D. N. Hendrickson and S. Hill, *Phys. Chem. Chem. Phys.*, 2009
DOI: 10.1039/b908460f

Spin-dynamics of the spin-correlated radical pair in photosystem I. Pulsed time-resolved EPR at high magnetic field
O. G. Poluektov, S. V. Paschenko and L. M. Utschig, *Phys. Chem. Chem. Phys.*, 2009
DOI: 10.1039/b906521k

Enantioselective binding of structural epoxide isomers by a chiral vanadyl salen complex: a pulsed EPR, cw-ENDOR and DFT investigation
Damien M. Murphy, Ian A. Fallis, Emma Carter, David J. Willock, James Landon, Sabine Van Doorslaer and Evi Vinck, *Phys. Chem. Chem. Phys.*, 2009
DOI: 10.1039/b907807j

Topology of the amphipathic helices of the colicin A pore-forming domain in *E. coli* lipid membranes studied by pulse EPR
Sabine Böhme, Pulagam V. L. Padmavathi, Julia Holterhues, Fatiha Ouchni, Johann P. Klare and Heinz-Jürgen Steinhoff, *Phys. Chem. Chem. Phys.*, 2009
DOI: 10.1039/b907117m

Structural characterization of a highly active superoxide-dismutase mimic
Vimalkumar Balasubramanian, Maria Ezhevskaya, Hans Moons, Markus Neuburger, Carol Cristescu, Sabine Van Doorslaer and Cornelia Palivan, *Phys. Chem. Chem. Phys.*, 2009
DOI: 10.1039/b905593b

Structure of the oxygen-evolving complex of photosystem II: information on the S_2 state through quantum chemical calculation of its magnetic properties
Dimitrios A. Pantazis, Maylis Orio, Taras Petrenko, Samir Zein, Wolfgang Lubitz, Johannes Messinger and Frank Neese, *Phys. Chem. Chem. Phys.*, 2009
DOI: 10.1039/b907038a

Population transfer for signal enhancement in pulsed EPR experiments on half integer high spin systems
Ilia Kaminker, Alexey Potapov, Akiva Feintuch, Shimon Vega and Daniella Goldfarb, *Phys. Chem. Chem. Phys.*, 2009
DOI: 10.1039/b906177k

The reduced [2Fe-2S] clusters in adrenodoxin and *Arthrospira platensis* ferredoxin share spin density with protein nitrogens, probed using 2D ESEEM
Sergei A. Dikanov, Rimma I. Samoilova, Reinhard Kappl, Antony R. Crofts and Jürgen Hüttermann, *Phys. Chem. Chem. Phys.*, 2009
DOI: 10.1039/b904597j

Frequency domain Fourier transform THz-EPR on single molecule magnets using coherent synchrotron radiation
Alexander Schnegg, Jan Behrends, Klaus Lips, Robert Bittl and Karsten Holldack, *Phys. Chem. Chem. Phys.*, 2009
DOI: 10.1039/b905745e

PELDOR study of conformations of double-spin-labeled single- and double-stranded DNA with non-nucleotide inserts
Nikita A. Kuznetsov, Alexandr D. Milov, Vladimir V. Koval, Rimma I. Samoilova, Yuri A. Grishin, Dmitry G. Knorre, Yuri D. Tsvetkov, Olga S. Fedorova and Sergei A. Dzuba, *Phys. Chem. Chem. Phys.*, 2009
DOI: 10.1039/b904873a

Site-specific dynamic nuclear polarization of hydration water as a generally applicable approach to monitor protein aggregation
Anna Pavlova, Evan R. McCarney, Dylan W. Peterson, Frederick W. Dahlquist, John Lew and Songi Han, *Phys. Chem. Chem. Phys.*, 2009
DOI: 10.1039/b906101k

Structural information from orientationally selective DEER spectroscopy
J. E. Lovett, A. M. Bowen, C. R. Timmel, M. W. Jones, J. R. Dilworth, D. Caprotti, S. G. Bell, L. L. Wong and J. Harmer, *Phys. Chem. Chem. Phys.*, 2009
DOI: 10.1039/b907010a

Structure and bonding of $[V^{IV}O(acac)_2]$ on the surface of AlF_3 as studied by pulsed electron nuclear double resonance and hyperfine sublevel correlation spectroscopy
Vijayasarathi Nagarajan, Barbara Müller, Oksana Storcheva, Klaus Köhler and Andreas Pöppl, *Phys. Chem. Chem. Phys.*, 2009
DOI: 10.1039/b903826b

Local variations in defect polarization and covalent bonding in ferroelectric Cu2+-doped PZT and KNN functional ceramics at themorphotropic phase boundary
Rüdiger-A. Eichel, Ebru Erünal, Michael D. Drahus, Donald M. Smyth, Johan van Tol, Jérôme Acker, Hans Kungl and Michael J. Hoffmann, *Phys. Chem. Chem. Phys.*, 2009
DOI: 10.1039/b905642d

Ferro- and antiferromagnetic exchange coupling constants in PELDOR spectra†

D. Margraf,‡[a] P. Cekan,‡[b] T. F. Prisner,*[a] S. Th. Sigurdsson*[b] and O. Schiemann*[c]

Received 18th March 2009, Accepted 1st June 2009
First published as an Advance Article on the web 29th June 2009
DOI: 10.1039/b905524j

Pulsed electron electron double resonance (PELDOR) is a well-established method for measuring nanometer distances between paramagnetic centres. Here, we demonstrate on three rigid and conjugated biradicals how the presence of an exchange coupling constant J and its distribtion ΔJ influences PELDOR data and its analysis. In principle two combinations of J and D fulfill the experimental data in each case. The correct one, including the sign of J, can be determined *via* simulations in case the two halves of the Pake pattern are separated enough.

1. Introduction

Pulsed electron–electron double resonance (PELDOR or DEER) is a well-established pulsed electron paramagnetic resonance (EPR) method for measuring distances between spin centres separated by up to 8 nm.[1] In addition to a single mean distance, a careful analysis of the modulation damping allows for an extraction of distance distributions that translate into dynamics at room temperature, as shown in combination with MD simulations for a range of rod-like acetylene–benzene systems.[2] Beyond distances, the number of interacting spins can be determined from the modulation depth[3] and recent PELDOR experiments performed at high-frequency/high-field revealed the possibility to determine angular information between cofactors fixed in their relative orientation by the protein scaffold.[4] For spin labels attached *via* a single bond the orientation information is blurred due to the inherent flexibility of the linker group.[5] This problem can be circumvented by connecting the label *via* two bonds and fusing it onto a conjugated ring system.[6] Such a label was recently used in oligonucleotides enabling the collection of angular information from X-band PELDOR data.[7]

Commonly, the PELDOR data are analyzed under the assumption that the isotropic exchange coupling constant J is negligible *versus* the anisotropic dipolar coupling ν_D and eqn (1) is used, with D being defined by eqn (2).

$$\nu_D = D(1 - 3\cos^2\theta) \quad (1)$$

$$D = \frac{\mu_0 h \gamma_A \gamma_B}{4\pi} \cdot \frac{1}{r^3} \quad (2)$$

μ_0 is the vacuum permeability, γ the magnetogyric ratios of spins A and B, h the Planck constant, r the distance between spins A and B, and θ the angle between r and the external magnetic field B_0. However, if J is non-zero, its inclusion into the PELDOR analysis by using eqn (3) instead of (1), may enable separating J from D and determining its magnitude and sign.

$$\nu_{AB} = \frac{\mu_0 h}{4\pi} \frac{\gamma_A \gamma_B}{r^3} (1 - 3\cos^2\theta) + J \quad (3)$$

In eqn (3), J is defined *via* the Hamiltonian $H_J = JS_AS_B$ and thus a positive value for J indicates an antiferromagnetic whereas a negative sign reflects a ferromagnetic coupling. Note that in contrast to the zero-field splitting constant, the dipolar coupling constant D is according to its definition in eqn (2) always positive.

Taking J explicitly into account may yield more accurate distances as well as information regarding the nature of the magnetic coupling. The latter is especially important for the design of molecular magnets.[8,9] Three examples have been reported in the literature where J has been included in the PELDOR analysis. A theoretical description with examples of molecules exhibiting very small exchange coupling constants were reported already in 1998[10] and later on for spin labeled copper(II)-porphyrin systems.[11] An early 3-pulse PELDOR experiment disentangled a J of 11 MHz.[12]

In order to investigate the effect of the sign and magnitude of J on PELDOR data and its analysis in more detail, we synthesized previously described biradical **1**[7] and two novel organic biradicals **2** and **3** (Scheme 1) using the same nitroxide as recently employed for oligonucleotide labeling.[6,7,13] To allow for antiferromagnetic and ferromagnetic exchange coupling, the two spin centres were connected *via* rigid and conjugated bridges, but with different substitution patterns.

2. Experimental

2.1 Synthesis

All air- or water-sensitive reactions were performed in flame-dried glassware under a positive pressure of argon. All commercial reagents were used without further purification.

[a] *Institute for Physical and Theoretical Chemistry, Centre for Biomolecular Magnetic Resonance, Goethe-University, Max-von-Laue-Str.7, 60438 Frankfurt, Germany. E-mail: prisner@chemie.uni-frankfurt.de*
[b] *Science Institute, University of Iceland, Dunhaga 3, 107 Reykjavik, Iceland. E-mail: snorrisi@hi.is; Fax: +354 552 8911; Tel: +354 525 4800*
[c] *Centre for Biomolecular Sciences, Centre of Magnetic Resonance, University of St. Andrews, North Haugh, St Andrews, UK KY 1619ST. E-mail: os11@st-andrews.ac.uk; Fax: +44 (0)1334 46 3410; Tel: +44 (0)1334 46 3410*

† Electronic supplementary information (ESI) available: NMR spectra, details of the simulations, determination of errors and detection pulse length variation for **2**. See DOI: 10.1039/b905524j

‡ Both D. Margraf and P. Cekan contributed equally to this work.

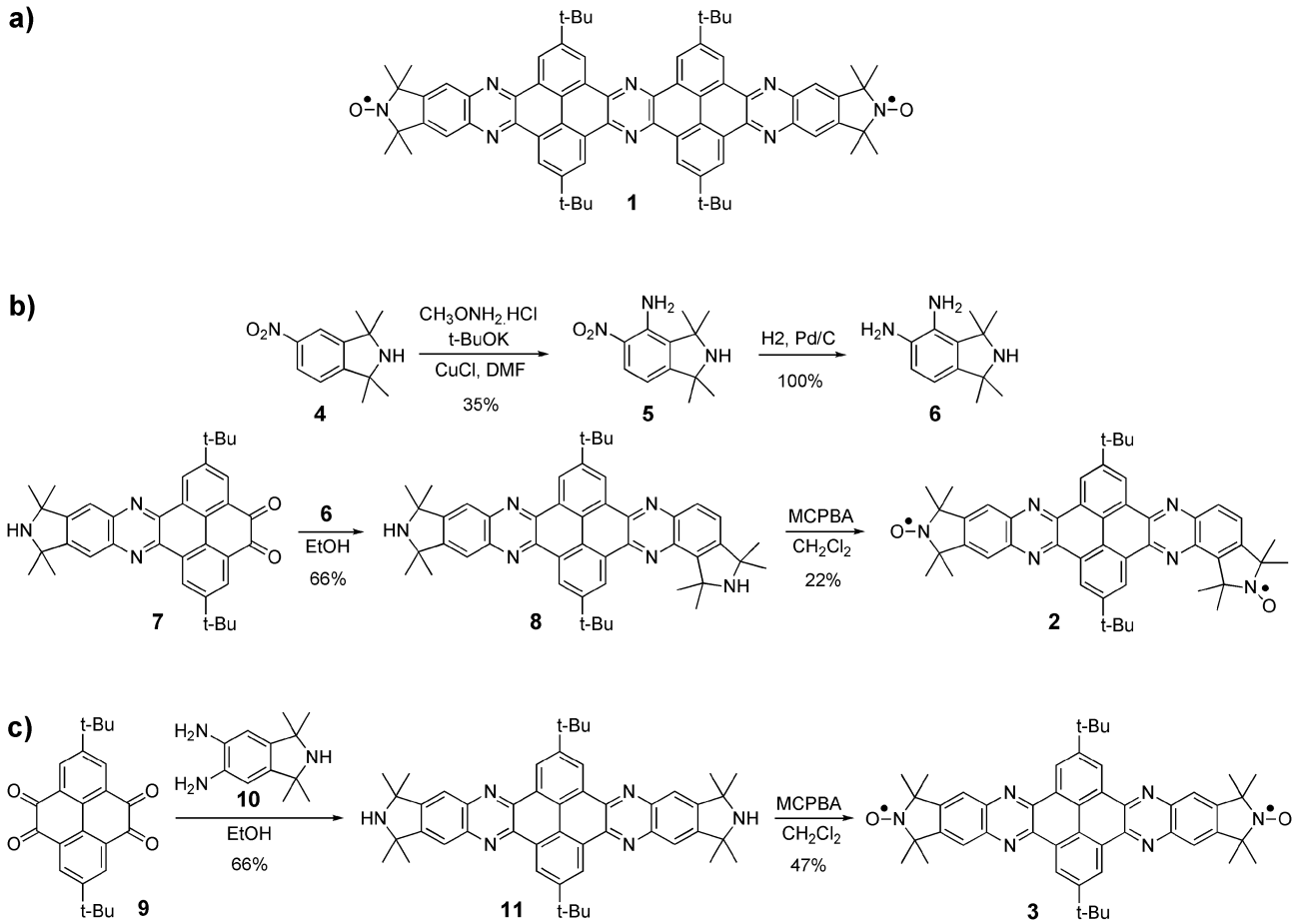

Scheme 1 (a) Structure of biradical **1**. Synthesis of (b) unsymmetric and (c) symmetric biradicals **2** and **3**, respectively.

CH_2Cl_2 was freshly distilled over calcium hydride under nitrogen. Water was purified on a MILLI-Q water purification system. Neutral silica gel (230–400 mesh, 60 Å) was purchased from Silicycle. Analytical thin layer chromatography (TLC) was performed on glass plates (Silicycle, ultra pure silica gel, 60 Å, F_{254}). NMR spectra for all organic compounds, including the paramagnetic ones **1–3**, were recorded on an Avance 400 MHz Bruker NMR spectrometer and the chemical shifts were reported in parts per million (ppm) relative to the deuterated NMR solvent used [^{1}H-NMR: $CDCl_3$ (7.26 ppm); ^{13}C-NMR: $CDCl_3$ (77.00 ppm)]. Commercial grade $CDCl_3$ was passed over basic alumina, immediately prior to use. Molecular weight (MW) of organic compounds was determined by high resolution electrospray ion trap mass spectrometer (HR-ESI-MS) (Bruker, MicroTof-Q). Analytical HPLC was carried out with a Waters 590 pump, a Waters UV detector 440, and Waters refractometer detector 410 on Macherey-Nagel Nucleosil 50–10 columns.

Nitroamine 5. A solution of CH_3ONH_2·HCl (79 mg, 0.936 mmol) and **4** (165 mg, 0.759 mmol) in DMF (3 mL) was added dropwise to a stirred solution of *t*-BuOK (504 mg, 4.49 mmol) and CuCl (16 mg, 0.15 mmol) in DMF (5 mL) over 5 min at 22 °C. Formation of a deep red color was observed. After 32 h at 22 °C, aqueous solution of saturated NH_4Cl (5 mL) was added, the products were extracted with CH_2Cl_2 and purified by flash column chromatography using neutral silica gel (gradient 100 : 0 to 75 : 25, CH_2Cl_2 : MeOH) to yield **5** (68 mg, 35%) as yellow crystals. TLC (silica gel 20% MeOH–CH_2Cl_2), R_f (**4**) = 0.90, R_f (**5**) = 0.70. ^{1}H-NMR ($CDCl_3$): δ 1.39 (s, 6H, 2 × CH_3), 1.55 (s, 6H, 2 × CH_3), 1.91(bs, 1H, NH), 6.22 (bs, 2H, NH_2), 6.46 (d, J = 8.5 Hz, 1H, ArH), 8.06 (d, J = 8.5 Hz, 1H, ArH). ^{13}C-NMR ($CDCl_3$): 29.02, 31.13, 62.59, 62.97, 110.47, 127.01, 132.23, 133.28, 140.56, 157.39. HR-ESI-MS ($M+H^+$): calcd for $C_{12}H_{18}N_3O_2$ 236.1394, found 236.1382.

Amine 6. A solution of **5** (16 mg, 0.066 mmol) in MeOH (10 mL) containing 10% Pd/C (2 mg) was hydrogenated at 55 psi for 2 h. The reaction mixture was filtered through a pad of celite and the filtrate was concentrated *in vacuo* to yield **6** (14 mg, 100%) as a white solid. TLC (silica gel 20% MeOH–CH_2Cl_2), R_f (**5**) = 0.70, R_f (**6**) = 0.05. ^{1}H-NMR ($CDCl_3$): δ 1.45 (s, 6H, 2 × CH_3), 1.61 (s, 6H, 2 × CH_3), 3.41 (bs, 4H, 2 × NH_2), 6.47 (d, J = 7.8 Hz, 1H, ArH), 6.67 (d, J = 7.8 Hz, 1H, ArH). ^{13}C-NMR ($CDCl_3$): 29.29, 31.88, 62.62, 63.03, 112.12, 117.38, 130.07, 132.74, 130.30, 142.18. HR-ESI-MS ($M+H^+$): calcd for $C_{12}H_{20}N_3$ 206.1652, found 206.1651.

Unsymmetric decacycle 8. A solution of **7** (30 mg, 0.055 mmol) in EtOH (20 mL) was treated with solution of **6** (14 mg, 0.066 mmol) in EtOH (20 mL). After stirring at 22 °C for 24 h, the solvent was removed *in vacuo*. The product was purified by

flash column chromatography using neutral silica gel (gradient 0.3 : 100 : 0 to 0.3 : 90 : 10, TEA : CH_2Cl_2 : MeOH) to give **8** (26 mg, 66%) as a light yellow solid. TLC (silica gel 0.3% TEA/15% MeOH–CH_2Cl_2), R_f (**6**) = 0.05, R_f (**7**) = 0.90, R_f (**8**) = 0.20. ^{1}H-NMR ($CDCl_3$): δ 1.76 (d, J = 6.2 Hz, 36H, 12 × CH_3), 2.22 (s, 6H, 2 × CH_3) 7.68 (d, J = 8.6 Hz, 1H, ArH), 8.19 (s, 2H, 2 × ArH), 8.39 (d, J = 8.6 Hz, 1H, ArH), 9.79 (m, 4H, 2 × ArH). ^{13}C-NMR ($CDCl_3$): 30.88, 31.13, 31.78, 31.90, 32.04, 35.79, 35.96, 63.10, 121.24, 121.27, 124.42, 124.50, 125.69, 125.81, 129.48, 129.55, 129.59, 130.50, 133.96, 137.99, 140.48, 142.12, 142.24, 142.29, 142.37, 142.41, 142.58, 143.53, 148.38, 150.80, 150.96. HR-ESI-MS ($M + H^+$): calcd for $C_{48}H_{53}N_6$ 713.4326, found 713.4352.

Unsymmetric biradical 2. To a solution of **8** (13 mg, 0.018 mmol) in CH_2Cl_2 (2 mL) was added MCPBA (81.7 mg, 0.365 mmol, (purity 77%) and the reaction stirred at 22 °C for 10 min. Dimethyl disulfide (1 mL) was added and the solution cooled to −78 °C to precipitate MCBA and the remaining MCPBA. The precipitate was removed by filtration and washed with cold CH_2Cl_2 (−78 °C). The filtrate was concentrated *in vacuo* and the residue purified by flash column chromatography using neutral silica gel (gradient 100 : 0 to 95 : 05, CH_2Cl_2–MeOH) to yield **2** (3 mg, 22%) as yellow crystals. Further purification was carried out *via* HPLC in [hexane–ethyl acetate (10 : 1)] + 100% dichloromethane.

TLC (silica gel 4% MeOH–CH_2Cl_2), R_f (**8**) = 0.05, R_f (**2**) = 0.95. ^{1}H-NMR ($CDCl_3$): δ 1.79 (bs, 18H, 6 × CH_3), 9.82 (bs, 4H, 4 × ArH) ppm. HR-ESI-MS ($M + H^+$): calcd for $C_{48}H_{50}N_6O_2$, 743.4071, found 743.4075.

Symmetric decacycle 11. A saturated solution of **9** (87 mg, 0.234 mmol) in EtOH (100 mL) was rapidly mixed with an ethanolic solution of **10** (96 mg, 0.468 mmol, 50 mL of EtOH). After stirring at 22 °C for 15 h, the solvent was removed *in vacuo*. The product was purified by flash column chromatography using neutral silica gel (gradient 100 : 0 to 90 : 10, CH_2Cl_2 : MeOH) to yield **11** (110 mg, 66%) as light yellow crystals. TLC (silica gel 10% MeOH–CH_2Cl_2), R_f (**9**) = 0.95, R_f (**10**) = 0.05, R_f (**11**) = 0.50. ^{1}H-NMR ($CDCl_3$): δ 1.74 (s, 24H, 8 × CH_3), 1.76 (s, 18H, 6 × CH_3), 8.18 (s, 4H, 4 × ArH), 9.79 (s, 4H, 4 × ArH). ^{13}C-NMR ($CDCl_3$): 31.91, 32.24, 35.95, 62.85, 121.22, 124.29, 125.71, 129.54, 142.26, 142.42, 150.87. HR-ESI-MS ($M + H^+$): calcd for $C_{48}H_{53}N_6$ 713.4326, found 713.4303.

Symmetric biradical 3. To a solution of **11** (37 mg, 0.052 mmol) in CH_2Cl_2 (10 mL) was added MCPBA (325.7 mg, 1.038 mmol, (purity 55%)) and the reaction stirred at 22 °C for 10 min. Dimethyl disulfide (3 mL) was added and the solution cooled to −78 °C to precipitate MCBA and the remaining MCPBA. The precipitate was removed by filtration and washed with cold CH_2Cl_2 (−78 °C). The filtrate was concentrated *in vacuo* and the residue purified by flash column chromatography using neutral silica gel (gradient 100 : 0 to 95 : 05, CH_2Cl_2 : MeOH) to yield **3** (110 mg, 66%) as a yellow solid. Further purification was carried out *via* HPLC in [hexane–ethyl acetate (10 : 1)] + 100% dichloromethane. TLC (silica gel 5% MeOH–CH_2Cl_2), R_f (**11**) = 0.15, R_f (**3**) = 0.95. ^{1}H NMR ($CDCl_3$): δ 1.79, (bs, 18H, 6 × CH_3), 9.83 (bs, 4H, 4 × ArH). ^{13}C-NMR ($CDCl_3$): 31.89, 36.01, 124.97, 125.84, 129.46, 143.20, 143.23, 151.11. HR-ESI-MS ($M + H^+$): calcd for $C_{48}H_{50}N_6O_2H$, 743.4074, found 743.4047.

2.2 Molecular modelling

The distances between the spin centres were estimated in molecules **1–3** using a MM2 routine as implemented in *ChemOffice 6.0* from Cambridge Soft Corporation with a minimum RMS gradient of 0.1.

2.3 EPR sample preparation

Samples with volumes of 100 μL and concentrations of 100 μM were prepared either as solutions in d_8-toluene or molten *o*-terphenyl for continuous wave (CW)- and PELDOR measurements, respectively. CW-EPR samples were saturated with argon prior to use. Samples were rapidly frozen in liquid nitrogen for low temperature measurements.

2.4 EPR instrumentation, experiments and simulations

CW X-band EPR spectra were acquired on a Bruker ELEXSYS E500 CW X-band EPR spectrometer. The microwave frequency created with a Bruker microwave bridge ER041MR was measured by use of a Systron Donner (6054D) frequency counter. The magnetic field was measured with a Bruker gaussmeter (ER035M). All room temperature spectra were recorded using a standard rectangular Bruker EPR cavity (ER4102ST7934) at a quality factor Q of about 3000, with a sampling time of 40 ms, a microwave power of 1 mW and a modulation amplitude of 0.1 mT at a modulation frequency of 100 kHz.

All PELDOR spectra were recorded on a Bruker ELEXSYS E580 pulsed X-band EPR spectrometer with a standard flex line probe head housing a dielectric ring resonator (MD5 W1) equipped with a continuous flow helium cryostat (CF935) and temperature control system (ITC 502), both from Oxford instruments. The second microwave frequency was coupled into the microwave bridge by a commercially available setup (E580-400U) from Bruker. All pulses were amplified *via* a pulsed travelling wave tube (TWT) amplifier (117X) from Applied Systems Engineering. The resonator was over-coupled to a quality factor Q of about 50. PELDOR experiments were performed with the pulse sequence $\pi/2(\nu_A)$–τ_1–$\pi(\nu_A)$–$(\tau_1 + t)$–$\pi(\nu_B)$–$(\tau_2 - t)$–$\pi(\nu_A)$–τ_2–echo.[14] The detection pulses (ν_A) were set to 32 ns for both π and π/2 pulses and applied at a frequency 40 to 80 MHz higher than the resonance frequency of the resonator. The pulse amplitudes were chosen to optimize the refocused echo. The π/2-pulse was phase-cycled to eliminate receiver offsets. The pump pulse (ν_B) with a length of 12 ns was set at the resonance frequency of the resonator. The field was adjusted such that the pump pulse is applied to the maximum of the nitroxide spectrum, where it selects the central m_I = 0 transition of A_{zz} together with the m_I = 0, ±1 transitions of A_{xx} and A_{yy}. The pulse amplitude was optimized to maximize the inversion of a Hahn-echo at the pump frequency. All PELDOR spectra were recorded at 40 K with an experiment repetition time of 4.5 ms. For **1** and **3** a video amplifier bandwidth of 25 MHz and a video amplifier gain of

60 dB was used. The time window τ_1 was set to 136 ns, τ_2 to 2500 ns and the time increment Δt for the dipolar evolution to 12 ns. 2000 scans with 206 data points were accumulated giving an approximate measurement time of 3 h necessary to obtain a signal-to-noise ratio $> 200:1$. In the case of **2**, the video bandwidth was increased to 50 MHz and the detection pulse length decreased to 16 ns. Furthermore, the time increment Δt was decreased to 4 ns and τ_2 was shortened to 1000 ns. 1000 scans with 244 data points were accumulated. In all three cases proton modulation was suppressed by addition of 8 spectra of variable τ_1 with a $\Delta\tau_1$ of 8 ns.[15] For comparison with simulations the time traces were divided by a mono-exponential decay and normalized to the point $t = 0$.

PELDOR data are commonly analyzed using data inversion methods, like Tikhonov regularization.[16] However, up to now all these methods are based on the assumption of negligible exchange coupling and angular correlations. Thus, their application to the data here would lead to erroneous results. We have, therefore, chosen to simulate the experimental PELDOR time traces with a home-written Matlab® program, in analogy to a procedure described earlier.[10,11,17]

3. Results and discussion

3.1 Synthesis

In order to obtain well-defined coupling tensors, the stable biradicals were required to be rigid to minimize line broadening resulting from conformational flexibility. Furthermore, the intramolecular distance between the two spin centres should amount to approximately 2 nm to observe several PELDOR modulations within a relatively short time window. Moreover, at such distances a conjugated bridge is mandatory to mediate exchange coupling through the bond system. Finally, the model systems should be accessible from a small pool of building blocks and permit access to different substitution patterns. Therefore, we synthesized two nitroxide biradicals **2** and **3**, both fulfilling the aforementioned criteria, as well as the previously described reference molecule **1** not displaying any exchange coupling (Scheme 1).[7]

The synthesis of biradical **2** started with amination of nitroisoindoline **4**[18] by *o*-methylhydroxylamine under basic conditions to give nitroamine **5**,[19] which was reduced to yield amine **6** (Scheme 1). Condensation of diketone **7**[7] with **6** gave the unsymmetric decacycle **8**, which was subsequently oxidized with *meta*-chloroperbenzoic acid (MCPBA) to yield unsymmetric biradical **2**. Symmetric biradical **3** was prepared in a similar fashion by condensation of tetraketone **9** with an excess of **10**[7,20] to yield decacycle **11**, followed by oxidation with MCPBA to yield **3**. Modelling molecules **1–3** using a standard molecular modelling routine yielded the intramolecular spin–spin distances given in Table 1.

3.2 CW-EPR

The presence of the nitroxide functional group in all three compounds was verified *via* CW X-band EPR measurements at 294 K. The typical nitroxide radical spectra are depicted in Fig. 1 (a)–(c). None of the spectra exhibits a splitting as anticipated for the expected small exchange coupling constants *J*. However, **2** and **3** reveal, compared to reference system **1**, a line-broadening of 0.4 G and 0.3 G for the central $m_I = 0$ transition, respectively, which is attributed to the presence of a weak exchange coupling.

Table 1 Geometric and exchange coupling parameters for **1–3** as determined from simulating the PELDOR time traces using the values from the Fourier transformed spectra as initial guesses. r_{MM} is the distance derived from molecular mechanics simulations

Molecule	r_{MM}/Å[a]	r_{PELDOR}/Å[b,d]	φ (°)[b]	J/MHz[b]	ΔJ/MHz[b]
1	26.5	26.9(1)	90(15)[c]	0.0(1)	0.0(1)
2	18.5	18.2(4)	90(15)	−3.2(6)	±0.8(3)
3	20.1	19.9(4)	[e]	+2.5(5)	±1.7(4)

[a] Measured as the average over the N–to–N and O–to–O distances. [b] The number in brackets indicates the error in the last digits. [c] The error was deduced in one of our previous publications and is assumed to be the same for **2**.[7] [d] The error in *r* states an observable difference in the frequency. [e] In this case φ cannot be determined from the PELDOR data (see text).

3.3 PELDOR

In contrast to the CW EPR spectra, where the resolution of electron–electron spin–spin coupling is limited by the inhomogeneous line width, PELDOR recovers the homogeneous line width and allows for the observation of weaker electron–electron interactions.

PELDOR time traces of **1**[7]–**3** (Fig. 2) were recorded by placing the 12 ns pump pulse on the maximum of the nitroxide spectrum (Fig. 3a), exciting all orientations of the nitroxide with respect to the external magnetic field (Fig. 3b). The 32 ns long detection pulses correspond to an excitation bandwidth of 26 MHz,[21] which cause, compared to a width of 210 MHz

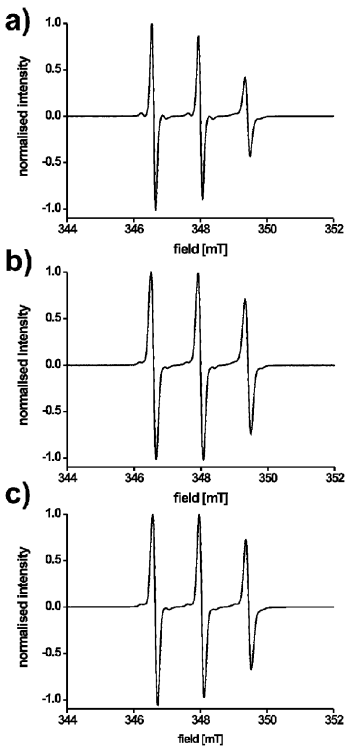

Fig. 1 CW X-band EPR spectra of (a) **1**, (b) **2** and (c) **3** recorded at room temperature.

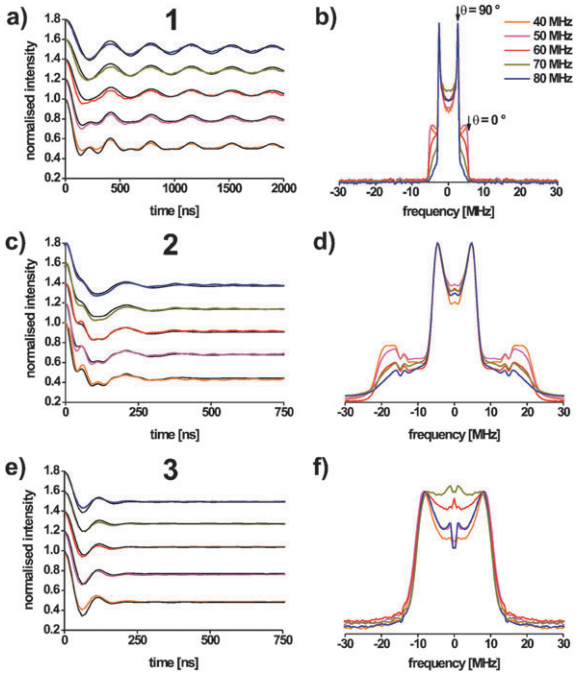

Fig. 2 Experimental PELDOR time traces recorded at different detection frequency offsets with simulations (parameters see Table 1) overlaid as black lines for (a) **1**, (c) **2** and (e) **3** shifted along the *y*-axis for better visibility. The corresponding Fourier transformed spectra are depicted in (b), (d) and (f) for **1**, **2** and **3**, respectively. The artefact at $\sim\pm14$ MHz in panel (d) is due to residual proton modulation caused by the short detection pulses.

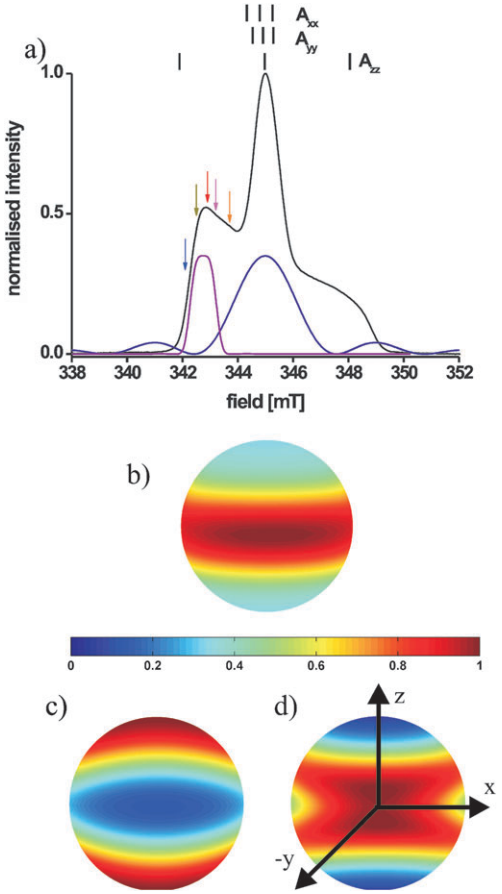

Fig. 3 (a) Field swept EPR spectrum of **1** at 40 K with the excitation profiles of the observer pulses (purple) and pump pulse (navy) and the corresponding ^{14}N stick spectrum. Arrows indicate observer pulse positions varying from $\Delta\nu$ = 40 MHz (orange) to 80 MHz (blue). Excited orientations for (b) the pump pulse and for the detection sequence with (c) $\Delta\nu$ = 80 MHz and (d) $\Delta\nu$ = 40 MHz. The intensities are normalised and colour coded, as indicated by the bar in (b).

for the nitroxide field swept spectrum, a selection of spectral components depending on the position of the detection sequence (Fig. 3c,d). Applying the detection pulses on the low-field edge of the spectrum (frequency offset $\Delta\nu = \nu_{detection} - \nu_{pump} = +80$ MHz) selects mainly the A_{zz} component of the ^{14}N-hyperfine tensor (Fig. 3c) whereas decreasing $\Delta\nu$ in steps of 10 MHz down to 40 MHz leads to an increased contribution of the A_{xx}, A_{yy} and off-diagonal components (Fig. 3d).

This translates into an orientation selection within the dipolar Pake pattern due to the rigid molecular frame of **1–3** fixing the orientation of the dipolar distance vector *r* with respect to the ^{14}N-hyperfine tensor. Since A_{zz} is fixed perpendicular to *r* in **1–3** ($\varphi = 90°$, see Fig. 5), the selection of A_{zz} leads for all three molecules to a selection of the perpendicular component ($\nu_{\perp}$,$\theta = 90°$) of the dipolar tensor. In turn, decreasing $\Delta\nu$ increases contributions of the parallel component ($\nu_{||}$, $\theta = 0°$). This can be followed in the PELDOR time traces of **1** (Fig. 2a) and more clearly in the Fourier transformed spectra (Fig. 2b). The geometric change induced by the different substitution pattern in **2**, affects only the orientation of A_{xx} and A_{yy} with respect to *r*, which is difficult to resolve at X-band frequencies. Thus, compared to **1**, the same trend regarding the orientation selection is observed in **2** (Fig. 2c,d). It should, however, be noted, that the broad width of this electron–electron coupling tensor prompted us to increase the video amplifier band width from 25 MHz to 50 MHz and to decrease the detection pulse lengths from 32 ns to 16 ns in order to circumvent frequency cut-offs by the amplifier and a too-narrow excitation band width of the detection pulses, respectively (see the ESI†). In addition, the dipolar evolution time increment Δt was reduced from 12 ns to 4 ns to obtain enough data points to clearly resolve a modulation period of $\sim$47 ns corresponding to a $\nu_{||}$ of 22.2 MHz. The pump pulse length of 12 ns, corresponding to an excitation bandwidth of 83 MHz, was short enough to fully excite the electron–electron coupling. In the case of molecule **3** (Fig. 2e and f), the orientation selection effect is less pronounced. The reason is that $\nu_{||}$ coincides with $\nu_{\perp}$, giving the same modulation frequency for either component. This prevents deriving a value for φ from the PELDOR data. The dependence of the modulation depth parameter λ on the fraction of molecules and orientations excited can, however, be seen for all three molecules.[22] The deepest modulation in each case is achieved for $\Delta\nu$ = 40 MHz, corresponding to a spectral position where all dipolar orientations are excited.

$$D[MHz] = \frac{\nu_{\perp} - \nu_{||}}{3} \quad (4)$$

$$J[MHz] = \frac{2\nu_{\perp} + \nu_{||}}{3} \quad (5)$$

Furthermore, the frequencies of the perpendicular and parallel singularities of the Pake pattern of **1** (Fig. 2b) can be read off as $\nu_{\perp} = 2.7$ MHz and $\nu_{||} = -5.4$ MHz. Substituting both values into eqn (4) and (5), derived from eqn (3),[12] yields $J = 0$ MHz and $D = 2.7$ MHz, which corresponds to an r of 26.8 Å according to eqn (2). However, the frequency of $\nu_{\perp}$ and $\nu_{||}$ could also be read off as -2.7 MHz and -5.4 MHz, respectively. With these values, one derives $J = -3.6$ MHz and $D = 0.9$ MHz ($r = 38.7$ Å). Fitting the time traces with both solutions as initial guesses clearly renders the former as correct (Fig. 4a and Table 1 for parameters. For details of the simulations see below and the ESI†). In this case it is easy to discriminate between both solutions since the latter pair with $r = 38.7$ Å and $J = -3.6$ MHz shifts the two halves of the Pake pattern far enough apart to create a hole in the spectral intensity around zero frequency which is clearly not present in the experiment. Also note the shift of the frequency in the simulated data due to the absence of the frequencies around zero MHz. The other two possibilities with $\nu_{||} = +5.4$ MHz and $\nu_{\perp} = \pm 2.7$ MHz, can be ruled out on the basis that D has to be positive.

In the case of molecule **2**, the presence of a non-zero J can be readily deduced from the broad width of the tensor (Fig. 2d). But also here two pairs of values can be determined for $\nu_{\perp}$ and $\nu_{||}$, $+4.6$ MHz and -22.2 MHz or -4.6 MHz and -22.2 MHz, respectively. The former pair yields $J = -4.3$ MHz and $D = 8.9$ MHz ($r = 18.0$ Å) and the latter $J = -10.5$ MHz and $D = 5.87$ ($r = 20.7$ Å). In this case it is already more difficult to select the correct solution, as the simulated time traces (parameters see Table 1) are not too far off the experiment for both pairs (Fig. 4b). Nevertheless, the pair with no hole between the two halves of the Pake pattern gives a better fit to the experiment (fitted values $J = -3.2$ MHz and $r = 18.2$ Å). In addition, this value for r is closer to the one from the molecular modelling (Table 1).

The Fourier transformed spectrum of **3** (Fig. 2f) can be rationalized as $\nu_{\perp} = 8.3$ MHz and $\nu_{||} = -8.3$ MHz or as $\nu_{\perp} = \nu_{||}$. The latter corresponds to a D approaching 0 MHz, r being very large, and $J = \pm 8.3$ MHz, which does not make sense. In the other case, realized in molecule **3**, r is 21.1 Å and J amounts to $+2.8$ MHz. *Via* simulations, it was not possible to differentiate between both solutions. The spectrum cannot be explained by a complete suppression of $\nu_{||}$ caused by orientation selection, since the variation of $\Delta\nu$ enables detecting all orientations as shown in Fig. 3c,d.

Independently from the PELDOR data, the cw EPR experiments confirm the presence of a small exchange coupling in molecule **2**, a slightly smaller one in **3** and its absence in **1** (see above).

In a more general way, in one solution J has to be large enough compared to D so that the hole between the two halves of the Pake pattern is broad enough. This may vary from sample to sample since the observation of a hole in the Pake pattern requires also a good knowledge of the intermolecular background.

The analysis laid out here relies on the assumption that the electron–electron coupling is not much larger than the frequency difference between the detected and pumped spins, which is full-filled even for $\Delta\nu = 40$ MHz for all three molecules. If the couplings were much larger, the Pake pattern would not contain any information on J and $\nu_{\perp}$ would appear at 1.5 times D.[1b]

Finally, the values obtained for r and J from reading-off the Fourier transformed spectra were substituted as initial guesses into the simulation program described earlier.[17] This program makes use of the spin Hamiltonian parameters, the experimental settings and geometric models based on the molecular structure (Fig. 5 and ESI†). These simulations yield the time traces in Fig. 2a,c,e and the data collected in Table 1, including the angle φ between A_{zz} and r for **1** and **2**, as well as distributions in r and J. The distributions are encoded in the modulation damping, the angle φ in the change of the orientation selection with $\Delta\nu$, and J and r in the frequency of the modulation. The distribution in J, ΔJ can be explained by the different molecular conformers, represented by the r-distribution, which will all give rise to slightly different orbital overlap. The values determined *via* the simulations are more precise than the ones determined from the Fourier transformations, since it is easier to fit the simulation to a repetitive pattern than to read-off the frequencies from a peak or edge.

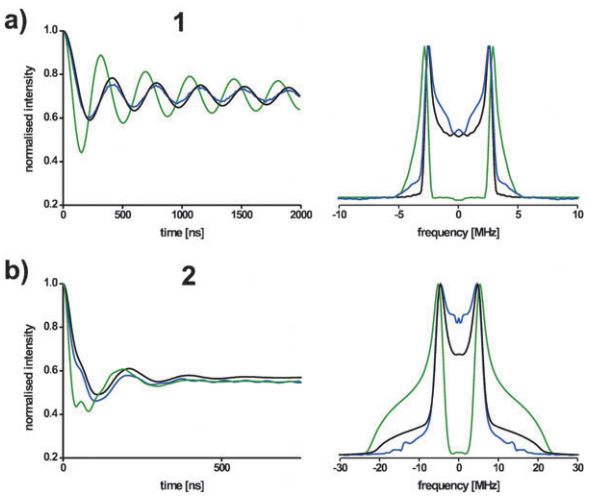

Fig. 4 Simulated time traces (see Table 1 for parameters) and FFTs for the two J/r pairs of a) molecule **1** (blue line: experiment; green line, wrong J/r pair with $J = -3.6$ MHz and $r = 38.7$ Å; black line, correct J/r pair with $J = 0$ MHz and $D = 2.7$ MHz) and (b) molecule **2** (blue line: experiment; green line, wrong J/r pair with $J = -10.5$ MHz and $r = 20.7$ Å; black line, correct J/r pair with $J = -4.3$ MHz and $r = 18.0$ Å). All for a frequency offset $\Delta\nu = 80$ MHz.

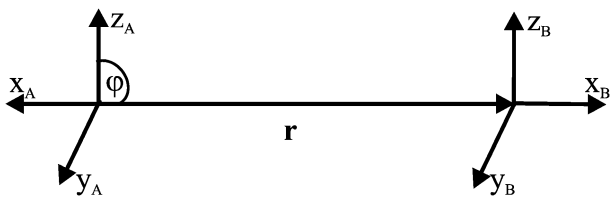

Fig. 5 Geometric model for **1**, **2** and **3** showing the A(^{14}N) axis system and the spin–spin distance vector.

4. Conclusions

We successfully synthesised two new model systems that display exchange coupling constants on the order of the dipolar coupling and recorded their 4-pulse PELDOR spectra. The rigidity of the molecules leads to angular correlations which can partially be resolved at X-band and analysed *via* the described simulation routine. In addition, the non-zero J yields two solutions for the J/r-couple and the correct one can be chosen based on simulations if the two pairs are different enough. For systems without conjugation in the interconnecting bridge this uncertainty is not critical, as the assumption of a negligible J is valid for the distance range accessible *via* PELDOR experiments. For molecule **2**, a ferromagnetic exchange coupling of $J = -3.2$ MHz was found, whereas an antiferromagnetic coupling of $J = +2.5$ MHz was determined for **3**. The change in the nature of the exchange coupling with respect to the substitution pattern may be rationalized by the exchange coupling pathways.

Acknowledgements

This work was supported by the Icelandic Research Fund (60028021), the Deutsche Forschungsgemeinschaft (SFB 579, RNA Ligand Interaction), the Centre for Biomolecular Magnetic Resonance and the EPSRC. P. Cekan thanks the Eimskip Fund of the University of Iceland for a doctoral fellowship and O. Schiemann acknowledges the Research Councils of the UK for a fellowship. We acknowledge Bela E. Bode for discussions.

References

1 (*a*) A. D. Milov, A. B. Ponomarev and Y. D. Tsvetkov, *Chem. Phys. Lett*., 1984, **110**, 67–72; (*b*) G. Jeschke, *Macromol. Rapid Commun*., 2002, **23**, 227–246; (*c*) O. Schiemann and T. F. Prisner, *Q. Rev. Biophys*., 2007, **40**, 1–53.

2 (*a*) A. Godt, M. Schulte, H. Zimmermann and G. Jeschke, *Angew. Chem*., 2006, **118**, 7722–7726 (*Angew. Chem., Int. Ed*., 2006, **45**, 7560–7654); (*b*) A. Marko, D. Margraf, H. Yu, J. Mu, G. Stock and T. F. Prisner, *J. Chem. Phys*., 2009, **130**, 064102, DOI: 10.1063/1.3073040.

3 (*a*) B. E. Bode, D. Margraf, J. Plackmeyer, G. Dürner, T. F. Prisner and O. Schiemann, *J. Am. Chem. Soc*., 2007, **129**, 6736–6745; (*b*) G. Hagelueken, W. J. Ingledew, H. Huang, B. Petrovic-Stojanovska, C. Whitfield, H. ElMkami, O. Schiemann and J. H. Naismith, *Angew. Chem. Int. Ed*., 2009, **121**, 2948–2950.

4 (*a*) V. P. Denysenkov, D. Biglino, W. Lubitz, T. F. Prisner and M. Bennati, *Angew. Chem*., 2008, **120**, 1244–1246 (*Angew. Chem., Int. Ed*., 2008, **47**, 1224–1227); (*b*) V. P. Denysenkov, T. F. Prisner, J. Stubbe and M. Bennati, *Proc. Nat. Acad. Sci. U. S. A*., 2006, **103**, 13386–13390; (*c*) A. Savitsky, A. A. Dubinskii, M. Flores, W. Lubitz and K. Möbius, *J. Phys. Chem. B*, 2007, **111**, 6245–6262.

5 Y. Polyhach, A. Godt, C. Bauer and G. Jeschke, *J. Magn. Reson*., 2007, **185**, 118–129.

6 N. Barhate, P. Cekan, A. P. Massey and S. Th. Sigurdsson, *Angew. Chem*., 2007, **119**, 2709–2712 (*Angew. Chem., Int. Ed*., 2007, **46**, 2655–2658).

7 O. Schiemann, P. Cekan, D. Margraf, T. F. Prisner and S. Th. Sigurdsson, *Angew. Chem. Int. Ed. Engl*., 2009, **121**, 3342–3345.

8 (*a*) A. Rajca, *Chem. Rev*., 1994, **94**, 871–893; (*b*) K. E. Vostrikova, *Coord. Chem. Rev*., 2008, **252**, 1409–1419; (*c*) D. M. Low, G. Rajaraman, M. Helliwell, G. Timko, J. van Slageren, R. Sessoli, S. T. Ochsenbein, R. Bircher, C. Dobe, O. Waldmann, H.-U. Güdel, M. A. Adams, E. Ruiz, S. Alvarez and E. J. L. McInnes, *Chem.–Eur. J*., 2006, **12**, 1385–1396; (*d*) S. J. Blundel, *Contemp. Phys*., 2007, **48**, 275–290.

9 (*a*) J. Fritscher, M. Beyer and O. Schiemann, *Chem. Phys. Lett*., 2002, **364**, 393–401; (*b*) C. Elschenbroich, M. Wolf, O. Schiemann, K. Harms, O. Burghaus and J. Pebler, *Organometallics*, 2002, **21**, 5810–5819; (*c*) C. Elschenbroich, O. Schiemann, O. Burghaus and K. Harms, *Chem. Commun*., 2005, 2149–2151.

10 (*a*) A. G. Maryasov, Y. D. Tsvetkov and J. Raap, *App. Magn. Reson*., 1998, **14**, 101–113; (*b*) A. D. Milov, A. G. Maryasov and Y. D. Tsvetkov, *Appl. Magn. Reson*., 1998, **15**, 107–143.

11 (*a*) B. E. Bode, J. Plackmeyer, T. F. Prisner and O. Schiemann, *J. Phys. Chem. A*, 2008, **112**, 5064–5073; (*b*) B. E. Bode, J. Plackmeyer, M. Bolte, T. F. Prisner and O. Schiemann, *J. Organomet. Chem*., 2009, **694**, 1172–1179. In these papers the sign of D has to be inverted, which has, however, no influence on the data.

12 A. Weber, O. Schiemann, B. Bode and T. F. Prisner, *J. Magn. Reson*., 2002, **157**, 277–285. In this paper, the signs of D and J have to be inverted.

13 P. Cekan, A. L. Smith, N. Barhate, B. H. Robinson and S. Th. Sigurdsson, *Nucleic Acids Res*., 2008, **36**, 5946–5954.

14 (*a*) R. E. Martin, M. Pannier, F. Diederich, V. Gramlich, M. Hubrich and H. W. Spiess, *Angew. Chem*., 1998, **110**, 2993–2998 (*Angew. Chem., Int. Ed*., 1998, **37**, 2833–2837); (*b*) O. Schiemann, N. Piton, J. Plackmeyer, B. E. Bode, T. F. Prisner and J. W. Engels, *Nat. Protoc*., 2007, **2**, 904–923.

15 G. Jeschke, A. Bender, H. Paulsen, H. Zimmermann and A. Godt, *J. Magn. Reson*., 2004, **169**, 1–12.

16 (*a*) G. Jeschke, G. Panek, A. Godt, A. Bender and H. Paulsen, *Appl. Magn. Reson*., 2004, **26**, 223–244; (*b*) M. K. Bowman, A. G. Maryasov, N. Kim and V. J. DeRose, *Appl. Magn. Reson*., 2004, **26**, 23–39; (*c*) Y. W. Chiang, P. P. Borbat and J. H. Freed, *J. Magn. Reson*., 2005, **172**, 279–295.

17 D. Margraf, B. E. Bode, A. Marko, O. Schiemann and T. F. Prisner, *Mol. Phys*., 2007, **105**, 2153–2160.

18 T. R. Miller and P. B. Hopkins, *Bioorg. Med. Chem. Lett*., 1994, **4**, 981–986.

19 S. Seko and N. Kawamura, *J. Org. Chem*., 1996, **61**, 442–443.

20 J. Hu, D. Zhang and F. W. Harris, *J. Org. Chem*., 2005, **70**, 707–708.

21 G. Jeschke, V. Chechik, P. Ionita, A. Godt, H. Zimmermann, J. Banham, C. R. Timmel, D. Hilger and H. Jung, *Appl. Magn. Reson*., 2006, **30**, 473–498.

22 R. G. Larsen and D. J. Singel, *J. Chem. Phys*., 1993, **98**, 5134–5146.

